MANSOURA JOURNAL OF CHEMISTRY
Official Journal of Faculty of Science, Mansoura University, Egypt
E-mail: scimag@mans.edu.eg ISSN: 2974-4938

Structure properties and adsorption capacity of 25wt. %SnO_2 /MCM-41 nanoparticles modified by phosphate ions

Sara I. I. El-Nagar, Wafaa S. Abo El-Yazeed, Awad I. Ahmed*

Chemistry Department, Faculty of Science, Mansoura University, Mansoura, Egypt

Received:12/1/2021
Accepted:24/1/2021

Abstract: Phosphated tin oxide-silica catalysts were synthesized by the sol-gel method using TEOS as silica source, CTAB as a surfactant, $SnCl_4.5H_2O$ as precursor, and H_3PO_4 in water as a modifier, followed by thermal treatment of the mixture. The composite exhibit a high adsorption capacity of brilliant green (BG) as a cationic organic dye. The sample was systematically characterized by XRD, TEM, and FT-IR techniques.

keywords: MCM-41, SnO_2, Adsorption capacity, Brilliant green dye, Sol-gel synthesis

1.Introduction

Nowadays the chemical industry to decrease the usage of dangerous environmentally chemicals facing a great challenge. Searching for a better method for chemical industries is become the center of this problem, and drawing a great attention to the scientist all over the world. Using solid acids catalyst is an important alternative to strategy of clean and safe process for environment greatest protection. Numerous types of binary mixed oxide systems have higher acid sites surface than single oxide [1]. Metal oxide-silica has lately drawn a lot of attention as it has acid strength more than alumina-silicates and yield positive results for several acid-catalyzed reactions[2].However, the formation mechanism of acid sites has not been properly comprehend still has suggested that Brønsted sites are produced on silica reached mixed oxides, as Kung Lewis sites predominates on metal oxide integrated samples with silica [3]. Tin oxide considers one of the greatest useful resources as its applications spotential, mostly the catalyst besides, carrier in maintained catalysts. As significant non-stoichiometry and crystal defects, tin oxide nanoparticles can be used more efficiently as a catalyst due to the faster

of the oxide ions within the SnO_2 nanoparticles to grow the surface to volume ratio [4]. Precipitation, sol-gel, hydrothermal, microwave-assisted syntheses, and ultrasonic spray pyrolysis are consider as several routes in chemistry that used to creating nanoparticles of mesoporous metal oxides as reported before [5]. But the most economical technique is sol-gel in mono- and poly component systems where it apposite to obtain the nanoparticles of metal oxide with high dispersion and limited size disaggregated, [6]. Otherwise, Si-MCM-41, have more orderly pore system for the coating metal species as SnO_2 nanoparticles which improved gases detect availability. Beside the sol-gel method was used to stabilize nano-sized SnO_2 particles on SiO_2 sheets by using encapsuling organic precursors in Si-MCM-41 pores using impregnation and chemical vapor deposition (CVD) techniques. The SnO_2 particles dimensional which detected using the sol-gel technique is located between 3 and 20 nm based on using acidic or basic path way. TEM, DR-UV/Vis. ,and adsorption isotherms' analysis confirming the two-dimensional of SnO_2 structure on the internal pores wall due to the strong interactions between the tin oxide species and the Si-MCM-41 silanol groups [7]. The wide bandgap tin dioxide semiconductor as a n-type, (E_g= 3.5 ~ 3.96 eV.), transparent to visible light. The tin dioxide-based materials have many potentials or demonstrated applications in various fields, as the converting of solar energy, encapsulating antistatic, catalysis, the sensing of gas, and the preparation of transparent electrode. Among these applications, semiconductor gas sensors based on Sn are appropriate instruments for detection of the inflammable or the toxic gases which diluted in air such as H_2, CH_4, N_2O,CO, H_2S, NO_2,in addition to methanol, and ethanol [8].A variation of catalysts which based upon tin compounds such as tin (II) (acetate, chloride, 2-ethyl hexanoate, and stearate) have been examined in the reactions of esterification and transesterification toward treating acid vegetable oils. All of these, otherwise tin (II) stearate, illustrate respectable catalytic activity in the transesterification reaction [9]. The single oxides altered (tin oxide silicate) within diverse anions such as SO_4^{2-}, PO_4^{3-}, WO_4^{2-}, F^-etc. improving the acidity and further physicochemical catalyst features as thermal stability, mesoporosity, etc. [10-12]. Nevertheless these anions altered metal oxides textural features are very poor as its low surface areas and the distributions of wide pore. While much stronger acid sites, have been required in chemical progressions, and it is desired to integrate more too stronger acid sites using alternating binary mixed oxides with anions. Lewis and Bronsted acidic sites were developed in anion modified metal oxide-silica mixed oxides [13-15]. The preparation method affected powerfully the acidity of systems. Phosphated metal oxides have attracted attention. As catalysts of phosphate-based solid acids have demonstrated quite effectiveness in numerous industrially imperative acid-demanding reactions.

2.Experimental

2.1 Materials

All reagents were utilized without further purification and were bought from Sigma-Aldrich.

The chemicals operated for the preparation of the catalysts are: tetraethyl orthosilicate (TEOS) (Si $(OC_2H_5)_4$, 99.0%, cetyl trimethyl ammonium bromide (CTAB), ammonia hydroxide solution (NH_4OH) 33%, tin chloride ($SnCl_4.5H_2O$), and orthophosphoric acid (H_3PO_4)98%.

2.2. Preparation of 35%PO_4^{-3}/25%SnO_2/ MCM-41 nanoparticles

The nanoparticles of SnO_2/MCM-41 was prepared using a sol-gel technique as reported before[16]. By dissolving 0.125gm $SnCl_4.5H_2O$ in 10 ml H_2O as metal oxide source then added to a suspension of 0.5 g. MCM-41 in 10 ml distilled water to form homogenous solution using magnetic stirrer after that drops wise of aqueous diluted ammonia was added until the formation of the white gel-like precipitate which was allowed to settle down for 2 hrs. and then continuously stirred for 30 min. The precipitate was filtered and dried at (60-80) overnight then the calcination of the precipitate was taken place at 550℃ in a muffle furnace to make sure of removal of all chloride ions as SnO_2 has thermal stability up to 500℃ and forming SnO_2/ MCM-41. Phosphate ions impregnated sample was obtained by mixing known amounts of calcinated SnO_2/MCM-41 sample with the appropriate amount of 3M H_3PO_4 in 10 mL distilled H_2O with stirring for 4 hrs. at room temperature. The mixture was kept for 48 hrs. to ensure that H_3PO_4 was completely adsorbed on SnO_2/ MCM-41 surface. The samples were calcined at 300 ℃ for 4 hrs. to remove unreacted phosphoric acid [17].

2.3 Techniques

2.3.1 X-ray diffraction analysis (XRD)

X-ray diffraction analysis of 35%PO_4^{-3}/25% SnO_2/MCM-41 sample was recorded at a high angle using PW 15 (Philips), and Cu Kα radiation source with Ni channel at a low and high point. The instrument was controlled at 40 kV and 45mA. The examination was made for 2θ point from 1 to 50 degrees, with a stage volume of 0.02 and step time of 2 seconds. Bragg's law and its association with the unit cell parameter are fused into conditions (2-1) and (2-2). Where the ordinary crystallite size of particles was constrained by XRD line augmenting strategy using Debye-Scherrer condition (2-3)

$$n\lambda = 2d_{100} \sin(\theta) \qquad (2\text{-}1)$$

$$a_o = \frac{2d_{100}}{\sqrt{3}} \qquad (2\text{-}2)$$

$$D = \frac{0.9\lambda}{\beta \cos\theta} \qquad (2\text{-}3)$$

where λ *is* radiation wavelength (Å), D is crystal size, θ = angle of reflection and β is the line breadth (radians) [18].

2.3.2. Transmission electron microscopy (TEM)

Transmission electron microscopy photograph and particle volume have gotten utilizing Jeol-Jem-2100 transmission electron microscope working at 120 KV. TEM tests were set up by soaking in a water suspension of proper sample powders onto a copper lattice enclosed which dried at a surrounding temperature and through holey carbon foil [19].

2.3.3. Fourier transform-infrared spectra (FT-IR)

Fourier transform-infrared spectrum of the prepared 35%wt.PO_4^{3-}/25%SnO_2 /MCM-41 nano sample was trailed by utilizing the in-situ FT-IR spectroscopic procedure on Nicolet Magna-IR 550 spectrometer through a 4cm^{-1}determination and 128 outputs in the mid-IR region 350-4000 cm^{-1}. The solid sample was crushed with KBr and hard pressed into a thin wafer which was set interior the IR cell and afterward the spectrum was recorded [20].

2.4. Adsorption activity of BG dye onPO_4^{3-}/25wt. %SnO_2 /MCM-41

Adsorption capacity of BG dye carried on system consist of 50 mL of BG dye with initial concentration 100 mg/L using 0.05 g/L of activated sample dose. The solution was stirred for 1 hour at 25°C and 250 rpm to get an adsorption/desorption stability. At given time intervals, 1.0 ml of the suspension was taken and centrifuged until the end of full separation. The remaining dye concentration was obtained by UV-visible spectrophotometer at a wavelength (λ_{max}) = 625 nm.). The adsorbed quantity of BG at stability (q_e mg/g), has been determined by the equation.

$$q_e = [(C_o - C_e)\,V]\;Wt \quad (2-4)$$

Where C_o is the initial concentration of BG dye (mg/l), C_e is the equilibrium concentration of BG dye (mg/l), V (L) is the volume of solution and wt. is the weight of the solid catalyst (g) [21]. Several adsorption effects such as contact time, initial concentration of BG dye, adsorbent weight, and calcination temperature have been studied BG dye.

3. Results and discussion

3.1. X-ray diffraction analysis

Figure1, shows the low X-ray diffraction lines of 35wt. %PO_4^{3-}/ 25% SnO_2/ MCM-41 sample calcined at 300 °C which indicates the presence of one reflection between 2ϴ = 0 to 10°. The position of the peak is 2ϴ = 2.345° (d = 37.67550 Å).

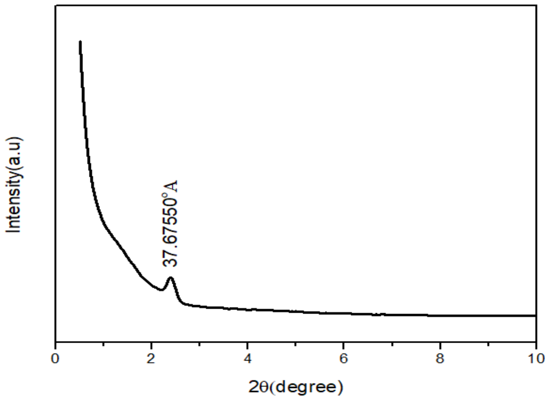

Fig.1. The low angle X-ray diffraction of 35wt. % PO_4^{3-}/ 25% SnO_2/ MCM-41

Which confirm the mesoporous hexagonal lattice of MCM-41. The low peak data confirm the formation of mesoporous MCM-41 sheets with super high crystallinity and porosity.

In Fig. (2), a strong intense peaks confirmed the tetragonal rutile structure of SnO_2 according to the standard XRD pattern [22]. The sharp and narrow peaks located at 2θ= 26.53, 34, 38, 51 .71, 54.75, 61.79, 65 and 65.8° indicate a high degree of crystallinity of SnO_2 in the nanocomposite [23]. This figure shows aboard hump in the range of 2$\boldsymbol{\theta}$=20-30° indicating the amorphous nature of MCM-41[24] due to the addition of SnO_2 to the support.

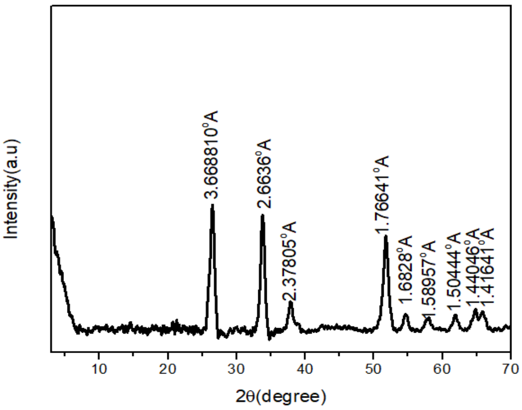

Fig.2. The wide-angle X-ray diffraction of 35wt. % PO_4^{3-}/ 25wt. % SnO_2/ MCM-41

No other peaks corresponding to the presence of phosphate is noticed that indicates PO_4^{3-} ions are incorporated into SnO_2 / MCM-

41 crystal lattice, or that PO_4^{3-} content is too little to be detected [25]. The higher intensities of the peaks resulted from the bigger grain size (10-30) nm in addition to better crystallinity of SnO_2. After loading PO_4^{3-} 35 wt. % onto 25 wt. % SnO_2 / MCM-41 the intensity of the peaks at $2\theta=26.53$, 34, 38, 51 .71, 54.75, 61.79, 65 and 65.8^{o} increases and the cell volume decrease. It seems that the incorporation of PO_4^{3-} into SnO_2 / MCM-41 crystal lattice as well as the increase of population of oxygen vacancies which may cause the distortion of the crystal lattice of parent 25% SnO_2 / MCM-41 sample [26]. The crystalline size (D) of 25%SnO_2 / MCM-41 was calculated using Scherrer equation, for the diffraction line located at $2\theta=26.47\ ^{o.}$ was found to be 22.1 nm which agrees with TEM results. While that for 35 % PO_4^{3-} 25wt. % SnO_2/ MCM-41 sample was found to be 19 nm.

3.2. Transmission electron microscopy (TEM)

TEM image confirmed that the homogeneous distribution of phosphate ions within the SnO_2/ MCM-41 nanosheets which approve that the impregnation technique is well-suited method for the modification of the surface of SnO_2/ MCM41 (Fig. 3). The results obtained agree well with XRD data.

3.3 Fourier transform-infrared spectra (FT-IR)

Figure (4) illustrates the FT-IR spectra of 35wt. % PO_4^{3-}/SnO_2/MCM-41. For MCM-41, abroad band appears at 1002-1259cm^{-1}owing to the Si-O-Si asymmetric stretching. The C-H vibrational stretching and O-H vibration bands appeared at 2923, 3450, and 1643 cm^{-1}[27]. The Si-O-Si rocking bending vibrational band appeared at 800 cm^{1}. The 479 cm^{-1} spectrum band appeared due to the vibrational bending of Si-O. FT-IR spectrum of SnO_2 thermally treated at 550^{o}C was detected in the 500- 700cm^{-1} range. Variation of spectrum bands is due to implications, and mixtures of OH, Sn–O, and Sn–O–Sn beings demonstrate in the 4000–800 cm^{-1}range; below 800 cm^{-1}there happens the inter ruptedimpacts of lattice vibrations. Because of discovering a suitable resolution in the region 400–1000cm$^{-1,}$ the IR spectrum of the solid sample hydroxyl appeared as a broad band and placed around 3430 cm^{-1}and a small band near1230 cm^{-1} are existing, which might be interpret by the existence of strongly bound hydroxyl groups which were condensed in the oxide bulk**.** To distinguish the vibrations due to OH. The spectrum region (800–1400 cm^{-1}) included most of FT-IR modes of ortho phosphoric acid. The P–O stretching region are ns P(OH)$_3$ at 890 cm^{-1}, n as P(OH)$_3$ at 1094 cm^{-1} (very poor), and n as(PO) at 971 cm^{-1}. The O PO$_3$ unit that occurs below 550 cm^{-1} may be at 468 cm^{-1} and the stretching modes of P–O spectrum over 750 cm^{-1} may be at 673 cm^{-1}[28].

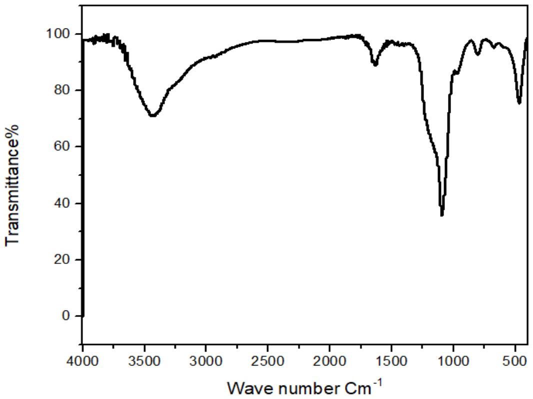

Fig.3. Fourier transform infrared spectra of 35wt. % PO_4^{3-}/ 25wt. % SnO_2/ MCM-41

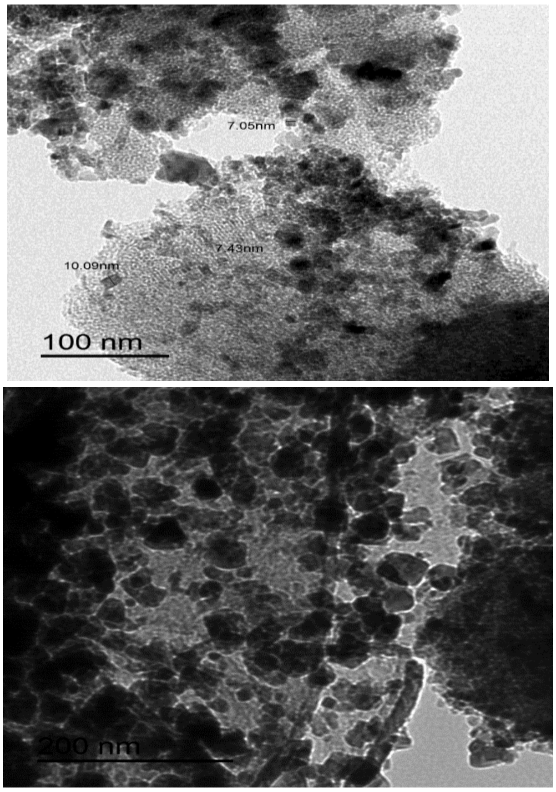

Fig 4. Transmission electron microscopy images of 35wt. % PO_4^{3-}/25wt. % SnO_2/ MCM-41

3.4. Adsorption capacity of 35%wt PO_4^{3-} /25%SnO_2/ MCM-41 for BG dye

3.4.1. Effect of contact time:

In figure (5) the removal rate of BG increases with the increase of contact time during the first 30 min then gradually increases to reach equilibrium after 60 min. This behavior was observed in the removal rate of BG dye on all calcinated samples.

3.4.2. Effect of Initial dye concentration:

Figure (6) indicates that the adsorption capacity of 35 wt. %PO_4^{3-}/SnO_2/MCM-41 sample decreases by increasing the initial dye. This might be resulted from the full saturation of the existing active sites of the adsorbent through the increase of initial dye concentration [29, 30].

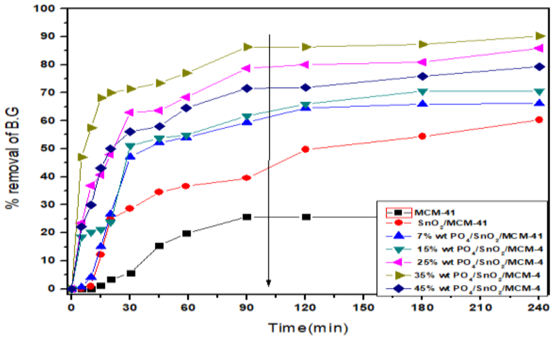

Fig 5: Contact time effect on BG dye adsorption

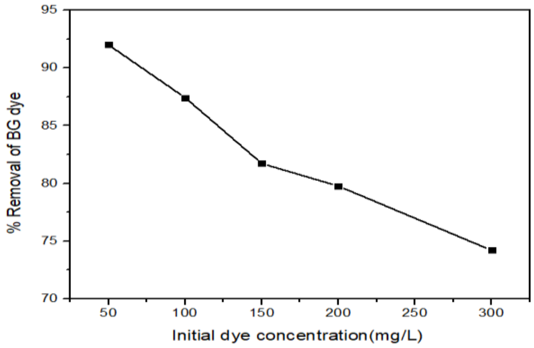

Fig 6 Initial BG concentration effect

3.4.3. Effect of calcination temperature:

Figure 7 indicates that the sample calcined at 300^0C show the highest adsorption activity. The decrease in percentage removal of the dye by increasing the calcination temperature up to 500 $^{\circ}$C might be result from a minor remaining quantity of template on the sample surface and /or due to the evaporation of a part PO_4 as a result of high temperature.

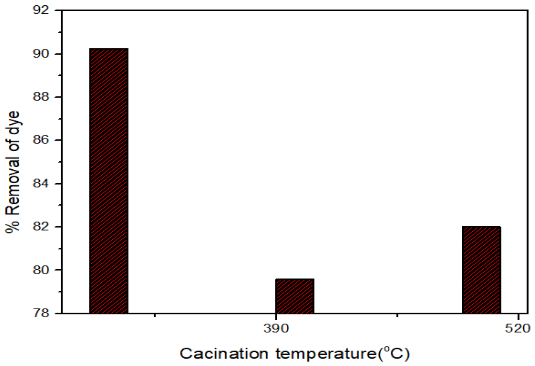

Fig 7 Effect of calcination temperature of 35wt . %PO_4^{3-}/ SnO_2/MCM-41 on % removal of BG dye

3.4.4. Effect of sample reuse

A slight decrease on the adsorption capacity was observed after reusing the sample 4 times at the same conditions. The % removal of BG dye using 35wt%PO_4^{3-}/SnO_2/MCM-41 was found to be 89.73, 81.70, 81.46, and 75.68% for 1, 2, 3, and 4 runs respectively. The FTIR spectrum of 35wt. %PO_4^{3-}/ 25wt%SnO_2/MCM-41 (Fig.8) show a slight difference between the fresh sample and those after recycling for three times, which indicates the high stability of the sample and its economical use .

3.4.5. Effect of catalyst doses

Sample weight was changed from 0.03 to 0.1g with keeping the dye initial concentration = 100 mg/L for 240 mins.Figure 9 indicates that the % removal of BG dye gradually increases from 70.85, to 90.23% by increasing the weight of sample from 0.03g to 0.1g .The increased removal at high dosage is expected due to the availabilty of more adsorption sites.

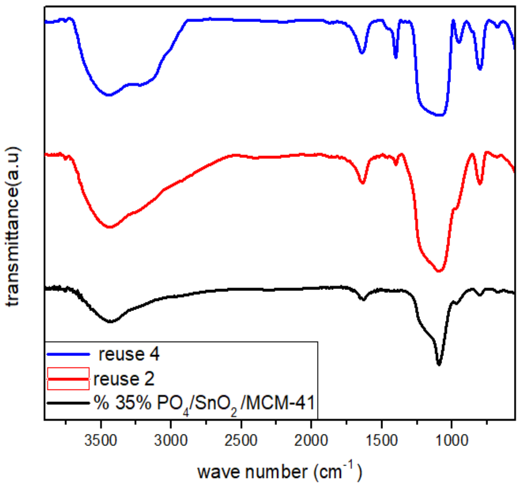

Fig.8 FT-IR of fresh and reusd sample.

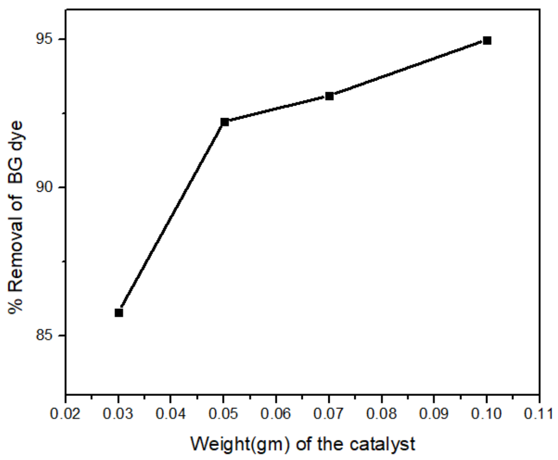

Fig 9: Sample dosage against % removal of BG.dye.

4. Conclusion

An eco-friendly phosphated tin oxide-silica catalyst was synthesized by using the sol-gel method for preparing tin oxide-silica catalyst followed by thermal treating at 550 °C .Then modified with phosphoric acid using impregnation method followed by 300 °C calcination temperature. The sample was characterized by XRD, TEM, and FT-IR techniques .The data demonstrated that 35wt. % $PO_4^{3-}/SnO_2/MCM$-41 possess a mesoporous nanosheets which displays ultrahigh absorbency and crystallinity. The % removal of BG dye was found influenced by loading phosphate ions on SnO_2/MCM-41, calcination temperature, initial dye concentration, and adsorbent doses. The highest adsorption capacity was obtained for the sample thermally treated at 300 °C.

4. Reference

1. Liu, N., et al., (2019). Metallic oxide-modified sulfated zirconia: an environment-friendly solid acid catalyst. New *Journal of Chemistry*, **43**(**8**): p. 3625-3632.
2. Wang, S., et al., (2020)Preparation of Biscuit-Like SO2− 4/ZrO2 Catalyst for Alkylation of o-Xylene with Styrene. *Journal of nanoscience and nanotechnology*,. **20**(**6**): p. 3496-3503.
3. Kalantar-zadeh, K., et al., (2016). Two dimensional and layered transition metal oxides. Applied Materials Today, **5**: p. 73-89.
4. Hassan, S., M. Mannaa, and A.A. Ibrahim(2019), Nano-sized mesoporous phosphated tin oxide as an efficient solid acid catalyst. RSC advances,. **9**(**2**): p. 810-818.
5. Zhu, J., B.Y. Tay, and J. Ma, (2006).Synthesis of mesoporous tin oxide on neutral surfactant templates. Materials Letters, **60**(**8**): p. 1003-1010.
6. Adnan, R., et al., (2010) Synthesis and Characterization of High Surface Area Tin Oxide Nanoparticles via the Sol-Gel Method as a Catalyst for the Hydrogenation of Styrene. *Journal of the Chinese Chemical Society*,. **57**(**2**): p. 222-229.
7. Moos, R. and K. Sahner, (2011) Chemical sensors based on zeolites.: Momentum Press: New York, USA.
8. Deng, H., (2004) Sol gel synthesis and characterization of tin oxide and doped-tin oxide nanosized materials used for gas-sensing., Marquette University.
9. Casas, A., et al., (2013)Tin compounds as Lewis acid catalysts for esterification and transesterification of acid vegetable oils. Fuel processing technology,. **106**: p. 321-325.
10. Lu, D., et al., (2016) Novel porous and hydrophobic POSS-ionic liquid polymeric hybrid as highly efficient solid acid catalyst for synthesis of oleate. Catalysis Communications,. **83**: p. 27-30.
11. Ahmed, A.I., et al., (2013).Characterization of 12-molybdophosphoric acid supported on mesoporous silica MCM-41 and its catalytic performance in the synthesis of hydroquinone diacetate. Applied surface science, **282**: p. 217-225.
12. Ahmed, A.I., et al., (2013).Nanostructure sulfated tin oxide as an efficient catalyst for the preparation of 7-hydroxy-4-methyl coumarin by Pechmann condensation reaction. *Journal of Molecular Catalysis A: Chemical*, **366**: p. 99-108.
13. Ryoo, R., (2019)Birth of a class of nanomaterial., Nature Publishing Group.
14. Kim, J.-Y. and O.-Y. Kwon, (2018)Preparation of Mesoporous Molecular Sieve by the Reaction of Na 2 SiO 3 and H 2 SiF 6 in the Presence of an Aqueous Nonionic Surfactant Solution.

Applied Chemistry for Engineering,. **29**(1): p. 122-126.

15. Xu, Y., et al., (2019) Nanoparticle-Encapsulated Hollow Porous Polymeric Nanosphere Frameworks as Highly Active and Tunable Size-Selective Catalysts. ACS Macro Letters,. **8**(10): p. 1263-1267.
16. Wang, H., et al., (2020). *I*solated Sn on mesoporous silica as a highly stable and selective catalyst for the propane dehydrogenation*.* **590**: p. 117291.
17. Fujihara, S., et al., (2004) Hydrothermal routes to prepare nanocrystalline mesoporous SnO2 having high thermal stability. Langmuir,. **20**(**15**): p. 6476-6481.
18. Ayyer, K., et al., (2016).Macromolecular diffractive imaging using imperfect crystals. Nature, **530**(7589): p. 202-206.
19. Al-Hada, N.M., et al., (2018) Thermal calcination-based production of SnO2 nanopowder: an analysis of SnO2 nanoparticle characteristics and antibacterial activities. Nanomaterials,. **8**(4): p. 250.
20. White, R., (2020)Chromatography/Fourier transform infrared spectroscopy and its applications.: CRC press.
21. Parida, K., K.G. Mishra, and S.K. Dash, (2012)Adsorption of toxic metal ion Cr (VI) from aqueous state by TiO2-MCM-41: Equilibrium and kinetic studies. *Journal of hazardous materials,*. **241**: p. 395-403.
22. Přech, J., M.A. Carretero, and J.J.C. Čejka, (2017) Baeyer–Villiger Oxidation of Cyclic Ketones by Using Tin–Silica Pillared Catalysts.. **9**(15): p. 3063-3072.
23. Inpasalini, M., et al., (2017)Influence of magnetic ion doping on structural, optical, magnetic and hyperfine properties of nanocrystalline SnO 2 based dilute magnetic semiconductors. *Journal of Materials Science: Materials in Electronics,*. **28(4)**: p. 3285-3292.
24. Zhang, S., et al., (2019) Investigation of the H2 sensing properties of multilayer mesoporous pure and Pd-doped SnO2 thin film. Sensors and Actuators B: Chemical,. **283**: p. 399-406.
25. Bose, K., R. Kesavan, and S. Deepa. (2020)Effect of dysprosium doping on the structural and gas sensing properties of SnO2 thin films. in AIP Conference Proceedings.. AIP Publishing LLC.
26. Jo, S.B., et al., (2020)Effects of Thin-Film Thickness on Sensing Properties of SnO2-Based Gas Sensors for the Detection of H2S Gas at ppm Levels. *Journal of Nanoscience and Nanotechnology,*. **20(11)**: p. 7169-7174.
27. Adrover, M.E., et al., (2020).Synthesis and characterization of mesoporous SBA-15 and SBA-16 as carriers to improve albendazole dissolution rate. Saudi *Pharmaceutical Journal*, **28(1)**: p. 15-24.
28. Lackey, H.E., et al., (2020) Reimagining pH Measurement: Utilizing Raman Spectroscopy for Enhanced Accuracy in Phosphoric Acid Systems. Analytical Chemistry,. **92(8)**: p. 5882-5889.
29. Boukoussa, B., et al., (2018) Adsorption behaviors of cationic and anionic dyes from aqueous solution on nanocomposite polypyrrole/SBA-15. *Journal of materials science,*. **53(10)**: p. 7372-7386.
30. Doğan, M., et al., (2004).Kinetics and mechanism of removal of methylene blue by adsorption onto perlite. *Journal of hazardous materials*, **109(1-3)**: p. 141-148.